Pedicle Drilling Planning Transfer for Spine Surgery Using Functional Map Correspondences

Lilyan Leblanc, Raphael Vialle, Cristina de Farias, E. Saghbini, Naresh Marturi, Brahim Tamadazte

▶ **To cite this version:**

Lilyan Leblanc, Raphael Vialle, Cristina de Farias, E. Saghbini, Naresh Marturi, et al.. Pedicle Drilling Planning Transfer for Spine Surgery Using Functional Map Correspondences. 2024 IEEE/RSJ International Conference on Intelligent Robots and Systems (IROS 2024), IEEE, Oct 2024, Abu Dhabi, United Arab Emirates. hal-04661996

HAL Id: hal-04661996
https://hal.science/hal-04661996

Submitted on 25 Jul 2024

HAL is a multi-disciplinary open access archive for the deposit and dissemination of scientific research documents, whether they are published or not. The documents may come from teaching and research institutions in France or abroad, or from public or private research centers.

L'archive ouverte pluridisciplinaire **HAL**, est destinée au dépôt et à la diffusion de documents scientifiques de niveau recherche, publiés ou non, émanant des établissements d'enseignement et de recherche français ou étrangers, des laboratoires publics ou privés.

Pedicle Drilling Planning Transfer for Spine Surgery Using Functional Map Correspondences

L. Leblanc[1], R. Vialle[1], C. de Farias[2], E. Saghbiny[1], N. Marturi[2], and B. Tamadazte[1]

***Abstract*— Precise pedicle screw placement is crucial in spine surgery, where minor inaccuracies can result in significant complications. Despite introducing robot-assisted navigation systems to aid surgeons, accommodating the spine's non-rigid movements (due to patient movement or interactions with the surgeon) often necessitates repeated intraoperative imaging, leading to increased radiation exposure. To address this challenge, we propose a novel method that utilizes the functional map (FM) framework to transfer drilling trajectories from preoperative CT scans to partially observed and noisy spine models. Specifically, the FM correspondences enhance the registration quality of pre-operative and perioperative 3D spine model data, even in the presence of non-rigid deformations. Through comprehensive simulations, we assess the method's effectiveness across various cases of complex deformations using a spine model consisting of five lumbar vertebrae obtained through CT scans. Validation involves evaluating registration errors in translation and rotation and verifying the clinical validity of transferred drilling trajectories. The results demonstrate the method's efficiency in transferring drilling trajectories onto noisy, partially observed, and deformed spine models.**

I. INTRODUCTION

Pedicle screw (PS) placement has become a standard surgical technique in spine surgery over the past few decades. It is extensively employed across various spinal procedures, notably in correcting spinal deformities such as scoliosis [1]. The surgical treatment, referred to as *arthrodesis*, involves spinal fusion achieved through the insertion of pedicle screws and correction with rods [2]. As shown in Fig. 1, the PS should be positioned correctly, *i.e.*, through the middle of the pedicle to obtain maximum stability of the bone-screw interface. Failure to accurately position the PS can result in a medial breach during insertion, leading to perforation of the spinal cord [3], or a lateral breach causing injuries to major vessels such as the aorta or vena cava. The literature indicates a complication rate of up to 18% attributed to the mispositioning of pedicle screws [4]. Overall, this highlights that the success of spinal surgery depends substantially on the safe and accurate positioning of the PS.

Drilling pedicles for screw placement presents a notable challenge, traditionally reliant on the surgeon's experience. However, technological advancements, such as navigation systems, robotic assistance, and augmented reality solutions, have become increasingly prominent. These innovations significantly enhanced accuracy and reduced complications. Navigation systems, for instance, locate surgical instruments in 3D and display them on pre- or intraoperative images, enabling surgeons to plan trajectories beforehand and navigate them during surgery. This involves mapping 3D insertion points and screw orientations onto each pedicle, necessitating precise pre- and intraoperative image registration [5]. Despite these advancements, spine surgery presents unique challenges. Spinal movement can induce variations from preoperative images throughout the procedure due to several factors. These include patient displacements (e.g., due to breathing), removal of muscle to access the pedicles during spine exposure, and the application of considerable forces during drilling trajectories. Moreover, while individual vertebrae are rigid, they can exhibit movement relative to each other, leading to spine deformation and complicating the registration process [6], [7]. Addressing these challenges is crucial for ensuring accurate surgical outcomes in spine-related procedures.

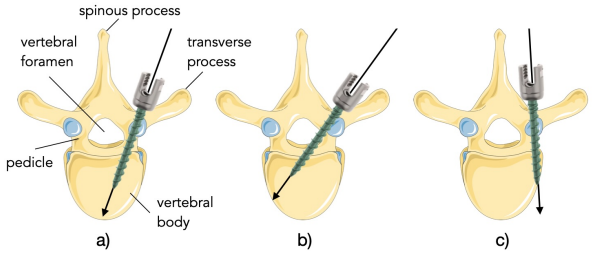

Fig. 1. Illustration of various screw placements in the vertebrae. a) Accurately positioned screw; b) medial perforation, which involves penetration into the spinal canal; and c) lateral perforation.

In robot-assisted spine surgery, managing spinal motion and accurately placing PS is crucial. The two most widely used methods to achieve this include employing per-operative CT scans and using optical trackers affixed to the patient's anatomy to compensate for patient motion (e.g., due to breathing). However, each has its drawbacks. CT scans offer detailed anatomical insights; nevertheless, frequent scans increase radiation exposure [8]. Conversely, although free from radiation risks, optical trackers cannot capture dynamic inter-vertebral deformations. An ideal solution would combine both benefits: a radiation-free approach that accurately captures the spine's deformations. Nonetheless, alternative radiation-free modalities such as depth cameras and ultrasound probes typically provide only partial views of the spine and can be obscured by noise. Consequently, under such challenging conditions of noisy and incomplete data, along

This work was supported by EU's H2020 research and innovation program under grant agreement No. 101016985 (FAROS. project)

[1]Sorbonne Université, CNRS UMR 7222, Inserm U1150, ISIR, F-75005, Paris, France. [2]Extreme Robotics Laboratory, School of Metallurgy and Materials, University of Birmingham, Edgbaston, B15 2TT, UK. leblanc@isir.upmc.fr

with the inter-vertebral movements, traditional geometric registration methods may struggle [9]. Recently, advancements in deep learning have shown potential in overcoming these challenges [10]. However, they require extensive training periods and sizable datasets, often unavailable or easily accessible.

In this work, we leverage the functional maps (FM) framework [11]–[13] to enhance the registration of pre-operative and perioperative 3D data. We aim to transfer the planned pedicle drilling trajectory from the pre-operative CT-scan model, *i.e.*, the drilling point and orientation, to an intraoperative model that often presents challenges due to being partial of lower quality and impacted by noise and deformations. Specifically, an initial FM is generated using rough manual landmarks on the vertebrae spinous process. This FM is refined through up-scaling to provide continuous and precise mapping, mainly to handle symmetries in the spine model. Finally, to individually register the segmented vertebrae, we apply the M-estimator sample consensus (MSAC) [14]. The resulting rigid transforms transfer drilling trajectories defined on the source (pre-operative) spine model to the target (per-operative) spine model. The quality of registration is evaluated both quantitatively and qualitatively:

(i) Quantitative evaluation is performed by computing the linear and angular registration errors using the Root Mean Squared Error (RMSE) metric. These errors are computed for each vertebra.

(ii) Qualitative evaluation is performed by evaluating whether the drilling trajectories are still clinically valid once transferred to the target spine model. Clinical validity is defined by the absence of lateral or medial breaches, as depicted in Fig. 1.

We have evaluated the effectiveness of our proposed approach across various challenging scenarios, including arbitrary deformation and partial data. For this purpose, we used a spine model composed of five lumbar vertebrae obtained through CT scans. In over 90 scenarios, totaling 900 drilling trajectory transfers, our method demonstrated an average linear RMSE of $0.94\,\mathrm{mm}$ and an average angular error of $1.32\,^\circ$. 900 out of 900 (100%) resulted in clinically valid drilling trajectories. These assessments encompass both best and worst-case scenarios. For best-case scenarios, errors are nearly negligible, with minimum linear and angular errors are $0.006\,\mathrm{mm}$ and $0.007\,^\circ$, respectively, resulting in 100% accuracy in trajectory transfer. On the other hand, for the worst-case scenario, which is characterized by noisy and partial data, the maximum linear and angular RMSE errors reach $2.34\,\mathrm{mm}$ and $2.54\,^\circ$, respectively, resulting in 100% accuracy in trajectory transfer.

II. PROBLEM STATEMENT

A drilling trajectory is defined by an entry point and exit point. The entry point of the pedicle screw is established at the intersection of either the pars interarticularis, mamillary process, lateral border of the superior articular facet, or mid-transverse process. The exit point is chosen to ensure the screw traverses the center of the pedicle's narrowest section, as shown in Fig. 2. Typically, the width of the pedicle screw (w_s) is 5 to $6\,\mathrm{mm}$. The narrowest part of the pedicle is encountered at a depth d_p of about $20\,\mathrm{mm}$ (of drilling) from the entry point. At this narrowest point, the width of the pedicle (w_p) measures roughly $11\,\mathrm{mm}$ for lumbar vertebrae [15]. Assuming the screw is precisely centered within the pedicle, on average, there will be a margin $l_m = \frac{w_p - w_s}{2}$ of about $2.5\,\mathrm{mm}$ between the screw and the pedicle's medial and lateral boundaries. Therefore, when transferring a drilling trajectory from a pre-operative scan to a per-operative model, the objective should be to limit the translational and rotational errors to a maximum of $\Delta_t = 2.5\,\mathrm{mm}$ and $\Delta_R = \mathrm{atan}(\frac{l_m}{d_p}) = 7.1\,^\circ$, respectively.

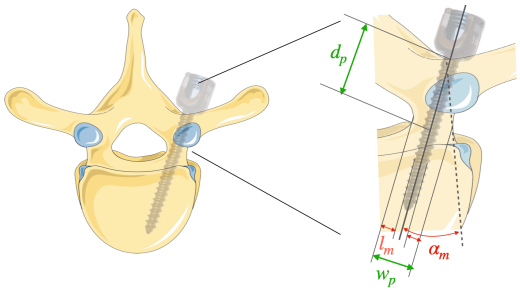

Fig. 2. Illustration of different margins during a pedicle screw placement.

III. TRAJECTORY TRANSFER METHODOLOGY

In this section, we present the FM framework and proceed with the developed pipeline for transferring pedicle drilling trajectories.

A. Functional Maps

The FM framework, introduced in [11] for the purposes of shape analysis and correspondence identification, serves as a tool for effectively transferring planned surgical trajectories. Previously, it has been used for various applications in computer graphics and, more recently, for robotic grasping [16]. The underlying idea behind the FM approach is that by reframing the shape-matching problem from a point-to-point search to feature correspondence within a more linear "functional space", it becomes simpler and more computationally efficient. In the context of transferring planned trajectories, such as pedicle screw trajectories from pre-operative to intraoperative spine models, the framework allows for the accurate mapping of crucial surgical points and orientations despite variations in shape or deformations.

Let $\mathcal{M}, \mathcal{N}$ be two shapes (source and target) represented by Riemannian manifolds with $n_\mathcal{M}$ and $n_\mathcal{N}$ their respective vertices. Let $\mathbf{T_P} : \mathcal{M} \rightarrow \mathcal{N}$ be the bijective point-wise mapping between $\mathcal{M}$ and $\mathcal{N}$. Directly optimizing over such correspondences leads to difficult, non-convex, non-linear optimization problems and becomes infeasible for dense point clouds or meshes. Instead, with the FM, shapes are encoded over a low-rank, compact basis for defining functions. Thus, a map within this framework includes pairings of real-valued functions rather than points [11]. In this manner, let $f : \mathcal{N} \rightarrow \mathbb{R}$ be a scalar function defined over $\mathcal{N}$. A corresponding scalar function $g : \mathcal{M} \rightarrow \mathbb{R}$ defined over

$\mathcal{M}$ is obtained by composition, *i.e.*, $g = f \circ \mathbf{T}_P$, with $\mathbf{T}_P$ being a map between the two shapes. This is denoted as the *functional representation* $\mathbf{T}_F$ of the mapping $\mathbf{T}_P$. It is worth noting that $\mathbf{T}_P$ matches points of shape $\mathcal{M}$ to points of shape $\mathcal{N}$ whereas $\mathbf{T}_F$ matches real-valued functions defined on $\mathcal{N}$ to real-valued functions defined on $\mathcal{M}$.

Next, let $\mathcal{M}$ and $\mathcal{N}$ be equipped with a set of orthogonal bases, $\{\phi_i\}$ and $\{\psi_i\}$ respectively. Then, the functions f and g can be represented as a linear combination $f = \sum_i a_i \psi_i$ and $g = \sum_i b_i \phi_i$. If $\{\phi_i\}$ and $\{\psi_i\}$ form orthonormal bases with respect to some inner product $\langle \cdot \ , \ \cdot \rangle$, then $f = \sum_i \langle f \ , \psi_i \ \rangle_{\mathcal{N}}$ and $g = \sum_i \langle g \ , \phi_i \ \rangle_{\mathcal{M}}$. From there, noting that T_F is a linear operator [11], we have

$$\begin{aligned} \mathbf{T}_F(\sum_i \langle f, \psi_i \rangle_{\mathcal{N}} \psi_i) &= \sum_i \langle f, \psi_i \rangle_{\mathcal{N}} \mathbf{T}_F(\psi_i) \\ &= \sum_{i,j} \langle f, \psi_i \rangle_{\mathcal{N}} \underbrace{\langle \mathbf{T}_F(\psi_i), \phi_j \rangle_{\mathcal{M}}}_{c_{ij}} \phi_j \quad (1) \end{aligned}$$

Truncating the series at the first k_n, k_m coefficients, one can obtain an approximation of $\mathbf{T}_F$, represented in the bases $\{\psi_i \ , \phi_i\}$ as a $k_n \times k_m$ matrix $\mathbf{C} = (c_{ij})$.

Now, let us assume that, through landmarks, segments preservation, and preserved functions, we have a set of q corresponding functions $\{f_1, ..., f_q\}$ and $\{g_1, ..., g_q\}$. Let $\mathbf{A}$ be the matrix representation of $a_{ij} = \langle f_i \ , \psi_j \ \rangle_{\mathcal{N}}$ for the first k_n bases and, similarly, $\mathbf{B}$ the matrix representation of $b_{ij} = \langle g_i \ , \phi_j \ \rangle_{\mathcal{M}}$ for the first k_m bases. Then, inferring functional correspondence reduces to solving a linear system of equations,

$$\mathbf{CA} = \mathbf{B} \quad (2)$$

Adequately choosing the bases $\{\phi_i\}$ and $\{\psi_i\}$ allows for a significant reduction in the size of this system, making it computationally efficient. If $q \geq k_{m,n}$, the system (2) is (over-)determined and is solved in the least squares sense to minimize the following energy

$$E_1(\mathbf{C}) = ||\mathbf{CA} - \mathbf{B}||^2 \quad (3)$$

Equation (3) presents the simplest optimization problem for recovering an unknown FM. Other regularization terms have been proposed to incorporate additional constraints, such as operator commutativity [11]–[13], local volume preservation and isometry [17], and descriptor-commutativity and orientation preservation [13]. Once an accurate FM is obtained, it is possible to retrieve the point-wise correspondence $\mathbf{T}_P$ [11].

B. Pipeline for Drilling Trajectory Transfer

The developed pipeline consists of the following key steps. First, drilling trajectories are defined on the source spine model, specifying entry points and drilling directions. Subsequently, new bases on both the source and target spine models are computed to facilitate the calculation of descriptor functions. These functions are crucial for enabling optimization within the FM framework. After mapping, $\mathbf{C}$ is derived and refined through iterative methods, it can be converted into a corresponding point-wise map. This conversion allows for the individual registration of vertebrae and the transfer of drilling trajectories from the source to the target models. All these steps are detailed below.

1) Compute the functional bases: We derive the *Laplace-Beltrami* eigenfunctions of $\mathcal{M}$ and $\mathcal{N}$ to serve as bases $\{\phi_i\}$ and $\{\psi_i\}$. This choice is common and particularly well-suited for shape-matching tasks, as these functions form an orthonormal basis, are invariant to isometric rigid motions, and are computationally tractable. Furthermore, eigenfunctions of the *Laplace-Beltrami* operator are ordered from "low frequency" to "higher frequency". Consequently, using only the first $k_n << n_{\mathcal{N}}, k_m << n_{\mathcal{M}}$ coefficients results in a 'low-pass' filtering effect, facilitating smooth correspondences. Typically, $k_n, k_m \in [20, 100]$ yields effective outcomes for shapes undergoing near-isometric deformations.

2) Compute global and local descriptors: We compute sets of descriptor vector functions f_i on $\mathcal{N}$ and g_i on $\mathcal{M}$ expressed as linear combination of the bases $\{\psi_i\}$ and $\{\phi_i\}$, respectively, and $\mathbf{C}$ satisfies $c_{i,j} f_i \approx g_i$. To this end, we combine global and local descriptors. Global descriptors are obtained using the Wave Kernel Signature (WKS) descriptor [18], which was proven efficient for a variety of datasets [19]. Local descriptors are obtained using the Heat Kernel Signature (HKS) descriptor [20] on landmarks manually selected on the top of the spine spinous process. WKS and HKS are invariant to isometry and are robust to some non-isometric deformations.

3) Estimate $\mathbf{C}$*:* Optimize $\mathbf{C}$ by minimizing an energy similar to E_1 given in (3). In this work, we adopt the approach presented in [13] to enhance the quality of the FM and to impose constraints ensuring approximate isometry and orientation preservation in the maps. This also incorporates a mask that promotes a slanted diagonal in $\mathbf{C}$, which is useful in the case of partial correspondences as shown in [21].

4) Refine $\mathbf{C}$ *and convert it to a point-wise mapping:* In challenging settings, *i.e.*, in the presence of noise, partiality and symmetries, it is useful to refine the obtained FM. This can be done by iterative alignment and refinement in the basis domain. Our implementation combines two refinement methods. Firstly, the Bijective and Continous ICP (BCICP) algorithm [19] improves the maps in the spatial and spectral domains. Specifically, our method can handle symmetries and noise. Finally, the *ZoomOut* algorithm [22] refines the FM through iterative spectral up-sampling, significantly improving the mapping precision. The conversion from the functional domain map ($\mathbf{T}_F$) to the point-wise mapping $\mathbf{T}_P$ is achieved using the same approach proposed by the original zoomOut method [22]. Examples of point-wise maps are shown in Fig. 5, where point correspondence is displayed as color correspondence.

5) Drilling trajectory transfer: Although the point-wise mapping $\mathbf{T}_P$ can directly transfer the drilling trajectories entry and exit points from a source spine model to a target spine model, local discontinuity in the map can lead to erroneous transfer. One possible solution is to utilize the nearest neighbors of the entry and exit points defined on the source spine model to filter out outliers on the corresponding points in the target spine model. In this work, knowing

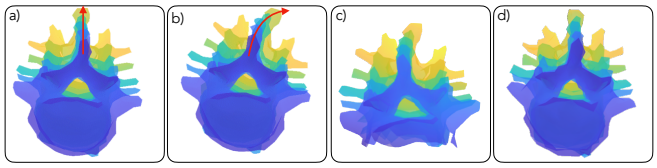

Fig. 3. The investigated cases of spine model deformation. a) and b) illustrate the spine model, obtained from a CT-scan, before and after non-rigid deformation, with each vertebra undergoing a cumulative rotation of $5°$ along the spine axis, as indicated by the red arrows. c) displays the removal of the lower half of the spine. d) exhibits the target model after adding a noise $\mathcal{N}(0,\, 1^2)$.

that individual vertebrae are anatomically rigid, we rely on segmenting the source spine model vertebrae. For each individual vertebra V_i, we extract the point cloud $\mathcal{M}_i$ on the source spine model and compute the corresponding point cloud on the target $\mathcal{N}_i$. Using the M-estimator sample consensus (MSAC) algorithm [14], we can then compute the optimal rigid transform $\mathbf{T}_{\mathcal{N}_i}^{\mathcal{M}_i} \in SE(3)$ between the two point clouds. It is important to note that for partial data, we use a rough segmentation of the upper half of the spine model, provided only to consider mapped points.

IV. EXPERIMENTAL RESULTS

In this section, we present the experiments conducted to evaluate the performance of our FM-based approach in transferring drilling trajectories. This transfer is performed from a source spine model to a target spine model that has undergone different deformations. The utilized source spine model consists of five lumbar vertebrae obtained through a CT scan. It measure approximately $180\,\mathrm{mm}$ in length, $80\,\mathrm{mm}$ in height and a vertebral body width of $45\,\mathrm{mm}$. To streamline the computational complexity, the original mesh of the source model containing more than 40,000 faces is simplified to approximately 3,500 faces. Two drilling trajectories were defined for each vertebra, corresponding to one per pedicle. Before the transfer process, individual vertebrae were manually segmented using the source spine model. Subsequently, we assign one approximate landmark per vertebra positioned atop the spinous process. The initial manual landmark alignment allows for pairings with a potential deviation of up to $5\,\mathrm{mm}$.

A. Investigated Cases

To assess the effectiveness of our approach, we registered a set of drilling trajectories, defined on a baseline spine model, onto modified versions of the spine model under challenging deformation scenarios. The following deformations, depicted in Fig. 3, have been tested.

1) Rigid deformation: A random rigid transform $\mathbf{T}^{\text{RAND}} \in SE(3)$ is applied to the entire spine model, *i.e.*, every point within the model undergoes the same rotation and translation. The linear components are randomly generated, i.e., $t_x, t_y, t_z \in [-2 \times M, +2 \times M]$ where M is the maximum dimension along x, y, and z axis of the spine model. Similarly, the angular components, $R_x, R_y, R_z \in [-30, +30]^\circ$ representing the Euler angles in the x, y, z directions are randomly generated.

2) Non-rigid deformation: Before applying $\mathbf{T}^{\text{RAND}}$ to the entire spine model, a distinct rotation $\mathbf{R}_i$ is applied to each vertebra. Specifically, the i^{th} vertebra, starting from the lowest one, undergoes a rotation of $(i-1) * 5$ degrees along the spine axis. This aligns with the understanding that vertebrae are anatomically rigid yet possess the ability to move slightly concerning each other, typically within a range of a few degrees [23]. This is shown in Fig. 3(a) and 3(b).

3) Partiality: Before applying $\mathbf{T}^{\text{RAND}}$ and $\mathbf{R}_i$, the lower half of the spine model is removed by a manual selection of the corresponding vertices. This approximates the expected view during an open surgery. It is depicted in Fig. 3(c).

In addition to the aforementioned cases, we evaluated our method's performance with clean and noisy data. For noisy cases, we applied a random Gaussian noise, $\boldsymbol{N} \sim \mathcal{N}(\boldsymbol{\mu}, \boldsymbol{\sigma}^2)$, to the model point cloud. For instance, with $\boldsymbol{N} \sim \mathcal{N}(0, 1^2)$, the added noise represents a data shift range of up to $6\,\mathrm{mm}$ (*i.e.*, $\pm 3\sigma$, a shift of 13% of the initial data smallest dimension). A comparison between clean and noisy models is shown in Fig. 3(a) and 3(d).

B. Drilling Trajectory Transfer Evaluation

In each deformation case, 10 registrations scenarios were computed, entailing the application of 10 different random deformations to the spine model. Vertebrae were registered individually between the source and target spine models. Subsequently, the linear and angular registration errors for each vertebra were evaluated using the RMSE metric. Additionally, qualitative analysis was performed by verifying the clinical validity of the transferred drilling trajectories on the target spine model. This involved checking for the absence of medial or lateral breaches, as illustrated in Fig. 1(b) and 1(c).

Detailed results are summarized in Table I. It includes RMSE registration errors for each vertebra and the overall percentage of clinically valid transferred drilling trajectories for each deformation scenario. Fig. 4 depicts a sample of the transferred planned drilling trajectories. In the figure, column 1 presents the trajectories planned on the pre-operative source model, and column 2 depicts the ground truth, representing pre-operative drilling trajectories perfectly transferred to the degraded target model. Column 3 shows the superposition of trajectories transferred to the target model using the ground truth transform (in blue) alongside those transferred using our approach (in red). Finally, column 4 presents the superposition of the ground truth trajectories (in blue) with the ones transferred with our method (in red) without the spine shape. For the best and worst-case scenarios, examples of point-wise maps are provided in Fig. 5, represented as colour correspondence.

C. Uniform Rigid Transform

When a single rigid transformation is applied to the entire spine model, our method yields perfect drilling trajectory transfer without noise. Furthermore, it consistently produced valid trajectories even in Gaussian noise, with a standard deviation of up to $1\,\mathrm{mm}$.

TABLE I

PERFORMANCE EVALUATION OF OUR DRILLING TRAJECTORY TRANSFER FOR DIFFERENT SPINE DEFORMATION SCENARIOS.

Type of data	Vertebra 1		Vertebra 2		Vertebra 3		Vertebra 4		Vertebra 5		Valid traj.
	$\Delta(\mathbf{t})^{\blacktriangle}$	$\Delta(\mathbf{R})^{\triangle}$	$\Delta(\mathbf{t})^{\blacktriangle}$	$\Delta(\mathbf{R})^{\triangle}$	$\Delta(\mathbf{t})^{\blacktriangle}$	$\Delta(\mathbf{R})^{\triangle}$	$\Delta(\mathbf{t})^{\blacktriangle}$	$\Delta(\mathbf{R})^{\triangle}$	$\Delta(\mathbf{t})^{\blacktriangle}$	$\Delta(\mathbf{R})^{\triangle}$	
Rigid deformation											
Clean*	0.007	0.005	0.005	0.003	0.001	0.002	0.010	0.012	0.004	0.006	100%
$\mathcal{N}(0,\, 0.5^2)$*	0.32	0.28	0.27	0.40	0.13	0.33	0.23	0.35	0.57	0.46	100%
$\mathcal{N}(0,\, 1^2)$*	1.21	1.17	0.52	0.75	0.49	0.94	0.60	0.89	1.20	1.08	100%
Mean†	**0.51**	**0.49**	**0.26**	**0.38**	**0.21**	**0.42**	**0.28**	**0.43**	**0.59**	**0.53**	**100%**
Non-rigid deformation											
Clean*	0.007	0.005	0.005	0.015	0.004	0.007	0.011	0.013	0.004	0.006	100%
$\mathcal{N}(0,\, 0.5^2)$*	0.48	0.41	0.25	0.39	0.12	0.37	0.24	0.33	0.38	0.38	100%
$\mathcal{N}(0,\, 0^2)$*	1.31	1.23	0.48	0.83	0.43	1.25	0.86	1.16	1.59	1.29	100%
Mean†	**0.60**	**0.55**	**0.25**	**0.41**	**0.19**	**0.54**	**0.37**	**0.50**	**0.66**	**0.56**	**100%**
Non-rigid deformation with partial data											
Clean*	0.16	0.00	0.13	0.01	0.16	0.30	0.16	0.00	0.16	0.00	100%
$\mathcal{N}(0,\, 0.5^2)$*	0.92	0.85	0.46	0.66	0.30	0.97	0.48	0.61	0.88	0.76	100%
$\mathcal{N}(0,\, 1^2)$*	3.37	3.04	1.23	1.83	1.45	4.39	2.01	4.83	2.90	2.71	100%
Mean†	**1.48**	**1.30**	**0.61**	**0.86**	**0.64**	**1.89**	**0.88**	**1.81**	**1.32**	**1.16**	**100%**

$^{\blacktriangle}$ Linear RMS error (in mm). $^{\triangle}$ Angular RMS error (in degrees). * 10 scenarios (100 trajectories) † 30 scenarios (300 trajectories)

D. Non-Rigid Transform

When applying cumulative rotations to every vertebra on top of a rigid transform to the entire spine, our method still yields promising results in noiseless cases. This highlights that the proposed method fully accommodates non-rigid deformations, provided they are isometric. Note that, although we selected a rotation angle of 5° for each vertebra to align with anatomical norms, empirical testing showed that the FMs could achieve accurate matching for rotation angles up to 25°. This indicates that the FM framework can handle a wide range of non-rigid transformations of considerable magnitude. Similarly to the rigid case, our FM-based method provides valid trajectories even in Gaussian noise, with a standard deviation of up to $1\,\mathrm{mm}$.

E. Data Partiality

In the presence of data partiality, a rough segmentation of the upper half of the spine model is provided only to account for the mapped points. In the absence of noise, our method still provides near-perfect results while only employing one rough landmark per vertebra. However, performance deteriorates rapidly in the presence of noise compared to the previous case. Results become unreliable when the standard deviation of the Gaussian noise reaches $2\,\mathrm{mm}$. In this case, manual inspection of the transferred trajectories revealed that most point-wise mappings are highly accurate, and most drilling trajectories are correctly transferred. However, isolated pairs of vertebrae registrations exhibited high errors. This indicates that both noise filtering and detection of highly discontinuous registration transforms between consecutive vertebrae could enhance the performance in the case of noisy scenarios.

F. Discussion

Initial results obtained with our FM-based framework are promising. Our method consistently provides accurate point-wise mappings even with only rough tuning of the FM parameters and one landmark pair per vertebra. Leveraging the rigidity of individual vertebrae, effective registration can be achieved for each vertebra, enabling efficient transfer of drilling trajectories between models. Remarkably, these results are achieved in just a few minutes per spine model using non-optimized Matlab code. We believe that efficient noise filtering could lead to significant improvements in handling noisy data. Additionally, while our approach successfully handled partial datasets, incorporating partial mesh completion techniques such as Gaussian Process Implicit Surfaces may prove beneficial when dealing with even more fragmented data, such as that obtained through RGB-D scans.

V. CONCLUSION

In this paper, we have presented a method for transferring drilling trajectories between spine models under different cases of deformations. Leveraging both the FM framework and anatomical knowledge of the spine, we have successfully transferred drilling trajectories from a clean CT scan of a spine model to noisy, partial, non-rigidly deformed versions of the spine model. While the initial results achieved with our method are promising, we believe that further investigation is necessary to gain a comprehensive understanding of the method's behavior. In this future direction, the spine database must first be expanded to further evaluate intra-spine and inter-spine registration. Furthermore, using multi-modal data (e.g., CT or ultrasound scans and RGB-D images) obtained on both ex-vivo and in-vivo cases is essential to better evaluate real-case surgical applications. Finally, exploring finer spine model meshes could enhance the point-wise correspondence obtained.

REFERENCES

[1] C. J. Hwang, J.-M. Baik, J. H. Cho, S. J. Yoon, *et al.*, "Posterior correction of adolescent idiopathic scoliosis with high-density pedicle

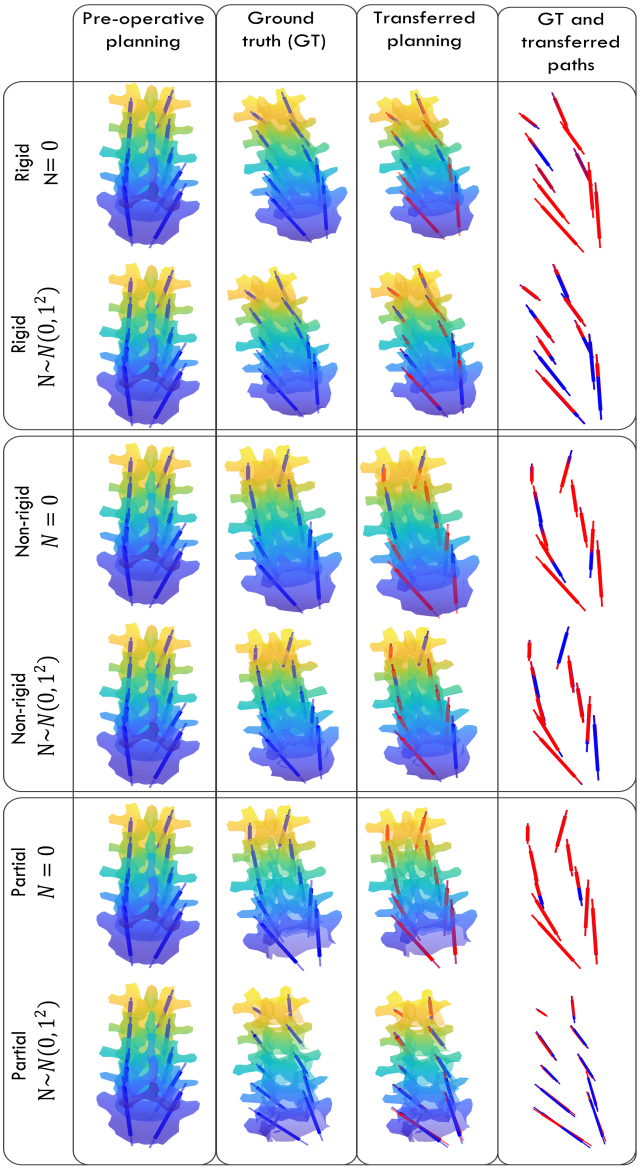

Fig. 4. Visualizing drilling trajectories transferred for various cases. 5 mm wide lines represent the trajectory. Column 1: Initial manual planning (blue) on a spine model. Column 2: Perfect transfer of drilling trajectories (blue) to the deformed spine model, serving as ground truth. Column 3: Deformed spine model with ground truth trajectories (blue) and those transferred using our FM-based method (red). Last column: Trajectories from column 3 displayed without the spine model for clarity. Trajectories color can overlap due to Z-fighting.

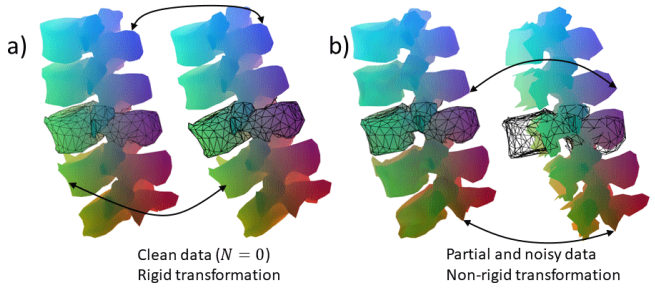

Fig. 5. Examples of point-wise mapping, represented as color correspondence, and individual vertebrae registration in black mesh. The source and target spine models are displayed on the left and right for each pair. a) Best case scenario (rigid transform without noise). b) Worst-case scenario (partial view, non-rigid deformation, noise $\mathcal{N}(0,\ 1^2)$.

screw-only constructs: 5 years of follow-up," *Yonsei Med. J.*, vol. 61, no. 4, p. 323, 2020.

[2] E. Cuartas, A. Rasouli, M. O'Brien, and H. L. Shufflebarger, "Use of all-pedicle-screw constructs in the treatment of adolescent idiopathic scoliosis," *J. of the Americ. Acad. of Orthop. Surg.*, vol. 17, no. 9, pp. 550–561, 2009.

[3] A. A. Faraj and J. K. Webb, "Early complications of spinal pedicle screw," *Euro. Spine J.*, vol. 6, pp. 324–326, 1997.

[4] J. Tang, Z. Zhu, T. Sui, D. Kong, *et al.*, "Position and complications of pedicle screw insertion with or without image-navigation techniques in the thoracolumbar spine: a meta-analysis of comparative studies," *J. of Biomed. Res.*, vol. 28, no. 3, p. 228, 2014.

[5] H. Esfandiari, C. Anglin, P. Guy, J. Street, *et al.*, "A comparative analysis of intensity-based 2d–3d registration for intraoperative use in pedicle screw insertion surgeries," *Int. J. of Comp. Ass. Rad. and Surg.*, vol. 14, pp. 1725–1739, 2019.

[6] J. R. Joseph, B. W. Smith, X. Liu, and P. Park, "Current applications of robotics in spine surgery: a systematic review of the literature," *Neurosurgical focus*, vol. 42, no. 5, p. E2, 2017.

[7] W. H. Shuman, A. A. Valliani, E. K. Chapman, M. L. Martini, *et al.*, "Intraoperative navigation in spine surgery: Effects on complications and reoperations," *World Neurosurgery*, vol. 160, pp. e404–e411, 2022.

[8] N. Fatima, E. Massaad, M. Hadzipasic, G. M. Shankar, *et al.*, "Safety and accuracy of robot-assisted placement of pedicle screws compared to conventional free-hand technique: a systematic review and meta-analysis," *The Spine J.*, vol. 21, no. 2, pp. 181–192, 2021.

[9] X. Huang, G. Mei, J. Zhang, and R. Abbas, "A comprehensive survey on point cloud registration," *arXiv preprint arXiv:2103.02690*, 2021.

[10] Z. Zhang, Y. Dai, and J. Sun, "Deep learning based point cloud registration: an overview," *Virt. Real. & Intel. Hard.*, pp. 222–246, 2020.

[11] M. Ovsjanikov, M. Ben-Chen, J. Solomon, A. Butscher, *et al.*, "Functional maps: A flexible representation of maps between shapes," *ACM Trans. on Graph.*, vol. 31, 07 2012.

[12] M. Ovsjanikov, E. Corman, M. Bronstein, E. Rodolà, *et al.*, "Computing and Processing Correspondences with Functional Maps," *ACM SIGGRAPH*, p. 63, 2017.

[13] J. Ren, M. Panine, P. Wonka, and M. Ovsjanikov, "Structured Regularization of Functional Map Computations," Wiley Online Library, pp. 39–53, 2019.

[14] P. H. Torr and A. Zisserman, "MLESAC: A New Robust Estimator with Application to Estimating Image Geometry," *Comput. Vis. and Image Underst.*, vol. 78, pp. 138–156, 2000.

[15] K. M. Ogden, C. Aslan, N. Ordway, D. Diallo, *et al.*, "Factors Affecting Dimensional Accuracy of 3-D Printed Anatomical Structures Derived from CT Data," *J. of Dig. Imag.*, vol. 28, pp. 654–663, 2015.

[16] C. De Farias, B. Tamadazte, R. Stolkin, and N. Marturi, "Grasp transfer for deformable objects by functional map correspondence," in *2022 International Conference on Robotics and Automation (ICRA)*. IEEE, 2022, pp. 735–741.

[17] R. M. Rustamov, M. Ovsjanikov, O. Azencot, M. Ben-Chen, *et al.*, "Map-based exploration of intrinsic shape differences and variability," *ACM Trans. on Graph.*, vol. 32, pp. 1–12, 2013.

[18] F. Tombari, S. Salti, and L. Di Stefano, "Unique signatures of histograms for local surface description," in *Computer Vision – ECCV*. Springer, 2010, pp. 356–369.

[19] J. Ren, A. Poulenard, P. Wonka, and M. Ovsjanikov, "Continuous and orientation-preserving correspondences via functional maps," *ACM Trans. Graph.*, vol. 37, pp. 1–16, 2018.

[20] J. Sun, M. Ovsjanikov, and L. Guibas, "A Concise and Provably Informative Multi-Scale Signature Based on Heat Diffusion," *Computer Graph. Forum*, vol. 28, no. 5, pp. 1383–1392, 2009.

[21] E. Rodolà, L. Cosmo, M. M. Bronstein, A. Torsello, *et al.*, "Partial Functional Correspondence: Partial Functional Correspondence," *Computer Graphics Forum*, vol. 36, no. 1, pp. 222–236, 2017.

[22] S. Melzi, J. Ren, E. Rodola, A. Sharma, *et al.*, "ZoomOut: Spectral Upsampling for Efficient Shape Correspondence," 2019.

[23] M. Kozanek, S. Wang, P. G. Passias, Q. Xia, *et al.*, "Range of Motion and Orientation of the Lumbar Facet Joints In Vivo:," *Spine*, vol. 34, no. 19, pp. E689–E696, Sept. 2009. [Online]. Available: http://journals.lww.com/00007632-200909010-00021